A collocated finite volume scheme to solve free convection for general non-conforming grids

Raphaele Herbin, Robert Eymard, Eric Chénier

A collocated finite volume scheme to solve free convection for general non-conforming grids

Eric Chénier *, Robert Eymard

Université Paris-Est, Laboratoire Modélisation et Simulation Multi Echelle, MSME FRE3160 CNRS, 5 bd Descartes, 77454 Marne-la-Vallée, France

Raphaèle Herbin

Université de Provence, 39 rue Joliot-Curie, 13453 Marseille, France

Abstract

We present a new collocated numerical scheme for the approximation of the Navier-Stokes and energy equations under the Boussinesq assumption for general grids, using the velocity-pressure unknowns. This scheme is based on a recent scheme for the diffusion terms. Stability properties are drawn from particular choices for the pressure gradient and the non-linear terms. Numerical results show the accuracy of the scheme on irregular grids.

Key words: Collocated finite volume schemes, general non-conforming grids, Navier-Stokes Equations, Boussinesq assumption

PACS: 65C20, 76R10

* Corresponding author.
Email addresses: Eric.Chenier@univ-paris-est.fr (Eric Chénier), Robert.Eymard@univ-paris-est.fr (Robert Eymard),

1 Introduction

Finite volume methods have been widely used in computational fluid dynamics for a long time; they are well adapted to the discretization of partial differential equations under conservative form, and one of their attractive features is that the resulting discretized equation has a clear physical interpretation [9]. In the framework of incompressible fluid flows, two strategies are often opposed, namely staggered and collocated schemes. The staggered strategy, which has become very popular since Patankar's book [9], remains mainly restricted to geometrical domains with parallel and orthogonal boundary faces. Therefore, for computations on complex domains with general meshes, the collocated strategy which consists in approximating all unknowns on the same set of points (called collocation points but also cell-centers or simply centers), is often preferred, even though the pressure-velocity coupling demands some cure for the stabilization of the well-known checkerboard pressure modes; to this purpose, various pressure stabilization procedures, based on improvements of the *Momentum Interpolation Method* proposed by Rhie and Chow [10], are frequently used [8]).

In [3,11], a collocated finite volume scheme for incompressible flows is developed on so called "admissible" unstructured meshes, that is meshes satisfying the two following conditions: the straight line joining the centers of two adjacent control volumes is perpendicular to the common edge, and the neighbouring control volumes and the associated centers are arranged in the same order, with respect to the common edge. Rectangular or orthogonal parallelepipedic meshes, triangular (2D) or tetrahedral (3D) Delaunay meshes, and Voronoi meshes fulfill these requirements. Under this assumption, the isotropic diffu-

Raphaele.Herbin@latp.univ-mrs.fr (Raphaèle Herbin).

sion fluxes can be consistently approximated by a two-point finite difference scheme. Using this approximation for a pure diffusion problem yields a symmetric "M-matrix" (which ensures monotony); the stencil is limited to the control volume itself and its natural neighbours and it leads to the classical 5- and 7-point schemes on rectangles and orthogonal parallelepipeds. Unfortunately, although the use of such grids considerably widens the variety of geometric shapes which can be gridded, it is far from solving all the critical needs resulting from actual problems:

- for complex 3D domains, to the large number of flat tetrahedra producing high discretization errors are often preferred generalized hexahedric meshes made of 3D elevations of quadrangular meshes, for which the faces of the control volumes are no longer planar;
- to our knowledge, there is yet no tool which is able to grid any geometrical shape in 3D using Voronoï or Delaunay tessellations, respecting the boundaries and the local refinement requirements;
- in compressible flows, the approximation of the full tensor by the usual two point scheme is no longer consistent even on admissible meshes, and multi-point approximations are therefore required;
- boundary layers are classically meshed with refined grids, so that the discretization scheme should be able to deal with non-conforming meshes.

Whereas there is no real difficulty to discretize the convective terms for general and non-conforming grids, the writing of accurate approximations of the diffusion contributions, particularly relevant for low Reynolds (Péclet) flows, is still a challenge on such meshes.

In the early 80's, Kershaw [7] first proposed a nine-point scheme on structured quadrilateral grids by using the restrictive assumption of a smooth mapping between the logical mesh and the spatial coordinates. Since then, numerous works have been published to efficiently solve the diffusion equations in general geometry (see [1] for a review of recent papers). The drawbacks of the actual schemes for diffusion are often linked with one or several of these key points:

- a non-local stencil (quite dense matrices);
- cell-centered but also face-centered unknowns (large matrices);
- non-symmetric definite positive matrices (loss of the energy balance);
- loss of the convergence or of the accuracy on some particular grids;
- loss of monotony for solutions in purely diffusive problems (the resulting matrix is not a "M-matrix").

We focus in this paper on the approximation of the Navier-Stokes and energy equations under the Boussinesq assumption, using a new scheme for diffusion terms. This scheme is shown to provide a cell-centered approximation with a quite reduced stencil, leading to symmetric definite positive matrices and to mathematical convergence proofs. Although the diffusion matrix is not known to satisfy the M-matrix property in general, the maximum principle was nevertheless preserved in our numerical three-dimensional simulations.

In this scheme, the discrete pressure gradient and the non-linear contributions are approximated so that the discrete kinetic and energy balances mimic their continuous counterparts. Indeed, the pressure gradient is chosen as the dual operator of the discrete divergence, and the discretization is such that there is no contribution of the non-linear velocity transport in the increase of kinetic energy. In order to suppress the pressure checkerboard modes, the mass bal-

ance is stabilized by a pressure expression which only redistributes the fluid mass within subsets of control volumes, the characteristic size of which is two or three times the local mesh size.

The remainder of this paper is divided into four sections. In section 2, the continuous formulation is presented in the framework of natural convection. The following section presents the discrete scheme and pays particular attention to the diffusive contribution. The fourth section is devoted to the numerical studies, first with analytical solutions and then for a natural convection problem.

2 Continuous formulation

Let d be the dimension of the space ($d = 2$ or 3) and let $\Omega \subset \mathbb{R}^d$ be an open polygonal connected domain. For $\boldsymbol{x} \in \Omega$, our aim is to compute an approximation of the velocity $\boldsymbol{u}(\boldsymbol{x}) = \sum_{i=1}^{d} u^{(i)}(\boldsymbol{x})\boldsymbol{e}_i$, the pressure $p(\boldsymbol{x})$ and the temperature $T(\boldsymbol{x})$, solution of the steady and dimensionless Navier-Stokes and energy equations under the Boussinesq approximation:

$$-\mathrm{Pr}\Delta\boldsymbol{u} + \boldsymbol{\nabla}p + (\boldsymbol{u}\cdot\boldsymbol{\nabla})\boldsymbol{u} - \mathrm{Ra}\,\mathrm{Pr}\,T\boldsymbol{e}_3 = \boldsymbol{f}(\boldsymbol{x}) \text{ in } \Omega \tag{1a}$$

$$-\Delta T + (\boldsymbol{u}\cdot\boldsymbol{\nabla})T = g(\boldsymbol{x}) \text{ in } \Omega \tag{1b}$$

$$\mathrm{div}\boldsymbol{u} = 0 \text{ in } \Omega \tag{1c}$$

where $\boldsymbol{e}_3$ indicates the vertical upward direction, $\boldsymbol{f}(\boldsymbol{x}) = \sum_{i=1}^{d} f^{(i)}\boldsymbol{e}_i$ and $g(\boldsymbol{x})$ are dimensionless regular functions modeling source or sink in the momentum or heat balances; Pr and Ra denote the Prandtl and Rayleigh numbers

respectively.

We consider the case of the homogeneous Dirichlet boundary conditions for the velocity and of the mixed Dirichlet- Neumann boundary conditions for the temperature. These boundary conditions read as follows:

$$\begin{cases} \boldsymbol{u}(\boldsymbol{x}) = \boldsymbol{0} & \boldsymbol{x} \in \Gamma, \\ T(\boldsymbol{x}) = T_b(\boldsymbol{x}) & \boldsymbol{x} \in \Gamma_1, \\ -\boldsymbol{\nabla} T(\boldsymbol{x}) \cdot \boldsymbol{n}(\boldsymbol{x}) = q_b(\boldsymbol{x}) & \boldsymbol{x} \in \Gamma_2, \end{cases} \tag{2}$$

where Γ denotes the boundary of the domain, $\Gamma_1, \Gamma_2 \subset \Gamma$ are such that $\Gamma_1 \cap \Gamma_2 = \emptyset$ and $\Gamma_1 \cup \Gamma_2 = \Gamma$, and $\boldsymbol{n}(\boldsymbol{x})$ is the outward unit normal vector to the boundary.

We assume that T_b is the trace on Γ_1 of a function, again denoted T_b, such that $T_b \in H^1(\Omega)$, and we define the functional space $H^1_{\Gamma_1,0}(\Omega) = \{T \in H^1(\Omega); T(\boldsymbol{x}) = 0 \text{ on } \Gamma_1\}$. Then a weak formulation of equations (1a-1c) with boundary conditions (2) reads: find $\boldsymbol{u} \in H^1_0(\Omega)^d$, $p \in L^2(\Omega)$ with $\int_\Omega p(\boldsymbol{x}) \mathrm{d}\boldsymbol{x} = 0$, and T with $T - T_b \in H^1_{\Gamma_1,0}(\Omega)$, such that

$$\begin{aligned} &\mathrm{Pr} \int_\Omega \boldsymbol{\nabla} \boldsymbol{u} : \boldsymbol{\nabla} \boldsymbol{v} \mathrm{d}\boldsymbol{x} - \int_\Omega p \, \mathrm{div} \boldsymbol{v} \mathrm{d}\boldsymbol{x} + \int_\Omega \mathrm{div}(\boldsymbol{u} \otimes \boldsymbol{u}) \cdot \boldsymbol{v} \mathrm{d}\boldsymbol{x} \\ &\quad - \mathrm{Ra}\,\mathrm{Pr} \int_\Omega T \boldsymbol{e}_3 \cdot \boldsymbol{v} \mathrm{d}\boldsymbol{x} = \int_\Omega \boldsymbol{f}(\boldsymbol{x}) \cdot \boldsymbol{v} \mathrm{d}\boldsymbol{x}, \ \forall \boldsymbol{v} \in H^1_0(\Omega)^d, \end{aligned} \tag{3a}$$

$$\begin{aligned} &\int_\Omega \boldsymbol{\nabla} T \cdot \boldsymbol{\nabla} \theta \mathrm{d}\boldsymbol{x} + \int_\Omega \mathrm{div}(\boldsymbol{u} T) \theta \mathrm{d}\boldsymbol{x} \\ &\qquad = \int_\Omega g(\boldsymbol{x}) \theta \mathrm{d}\boldsymbol{x} - \int_{\Gamma_2} q_b(\boldsymbol{x}) \theta(\boldsymbol{x}) \mathrm{d}\boldsymbol{x}, \ \forall \theta \in H^1_{\Gamma_1,0}(\Omega). \end{aligned} \tag{3b}$$

$$\mathrm{div}\boldsymbol{u}(\boldsymbol{x}) = 0 \text{ for a.e. } \boldsymbol{x} \in \Omega, \tag{3c}$$

Although we focus in this paper on finite volume schemes, the principles of the discretization are also much inspired by the weak form (3a-3c).

3 Numerical scheme

We denote by $\mathcal{D} = (\mathcal{M}, \mathcal{E}, \mathcal{P})$ a space discretization, where (see Fig. 1):

- $\mathcal{M}$ is a finite family of non empty connected open disjoint subsets of Ω (the "control volumes") such that $\overline{\Omega} = \cup_{K\in\mathcal{M}}\overline{K}$. For any $K \in \mathcal{M}$, let $\partial K = \overline{K} \setminus K$, $\mathrm{m}_K > 0$ and h_K respectively denote the boundary, the measure and the diameter of K.
- $\mathcal{E}$ is a finite family of disjoint subsets of $\overline{\Omega}$ (the "edges" of the mesh), such that, for all $\sigma \in \mathcal{E}$, σ is a non empty open subset of a hyperplane of $\mathbb{R}^d$, whose (d-1)-dimensional measure m_σ is positive. We assume that, for all $K \in \mathcal{M}$, there exists a subset $\mathcal{E}_K$ of $\mathcal{E}$ such that $\partial K = \cup_{\sigma\in\mathcal{E}_K}\overline{\sigma}$. We then denote by $\mathcal{M}_\sigma = \{K \in \mathcal{M}, \sigma \in \mathcal{E}_K\}$. The set $\mathcal{E}$ is assumed to be partitioned into $\mathcal{E} = \mathcal{E}_{\mathrm{int}} \cup \mathcal{E}_{\mathrm{ext}}$, such that, for all $\sigma \in \mathcal{E}_{\mathrm{ext}}$ (boundary edge), $\mathcal{M}_\sigma$ has exactly one element and $\sigma \subset \partial\Omega$, and for all $\sigma \in \mathcal{E}_{\mathrm{int}}$ (interior edge), $\mathcal{M}_\sigma$ has exactly two elements. We also assume that, if $\sigma \in \mathcal{E}_{\mathrm{ext}}$, then either $\sigma \subset \Gamma_1$ or $\sigma \subset \Gamma_2$. For all $\sigma \in \mathcal{E}$, we denote by $\boldsymbol{x}_\sigma$ the barycenter of σ. For all $K \in \mathcal{M}$ and $\sigma \in \mathcal{E}_K$, we denote by $\boldsymbol{n}_{K,\sigma}$ the unit vector normal to σ outward to K.
- $\mathcal{P}$ is a family of points of Ω indexed by $\mathcal{M}$ (the collocation points), denoted by $\mathcal{P} = (\boldsymbol{x}_K)_{K\in\mathcal{M}}$, such that for all $K \in \mathcal{M}$, K is assumed to be $\boldsymbol{x}_K$-star-shaped, which means that for all $\boldsymbol{x} \in K$, the property $[\boldsymbol{x}_K, \boldsymbol{x}] \subset K$ holds.

The Euclidean distance $d_{K,\sigma}$ between $\boldsymbol{x}_K$ and the hyperplane including σ is assumed positive. We then denote by $C_{K,\sigma}$ the cone with vertex $\boldsymbol{x}_K$ and basis σ, and by $\mathrm{m}_{K,\sigma} = \mathrm{m}_\sigma d_{K,\sigma}/d$ its measure.

For any edge $\sigma \in \mathcal{E}_{\rm int}$, we define a linear mapping $\Pi_\sigma : \mathbb{R}^{\mathcal{M}} \to \mathbb{R}$ (where an element $v \in \mathbb{R}^{\mathcal{M}}$ is defined by the family of real values $(v_K)_{K\in\mathcal{M}}$) such that for any regular function ψ, setting $v_K = \psi(\boldsymbol{x}_K)$ for all $K \in \mathcal{M}$, then $\Pi_\sigma(v)$ is a second order approximation of $\psi(\boldsymbol{x}_\sigma)$. In such a case, there exist coefficients $(\beta_\sigma^L)_{L\in\mathcal{M}}$ such that

$$\Pi_\sigma(u) = \sum_{L\in\mathcal{M}} \beta_\sigma^L u_L \text{ with } \sum_{L\in\mathcal{M}} \beta_\sigma^L = 1,\ \boldsymbol{x}_\sigma = \sum_{L\in\mathcal{M}} \beta_\sigma^L \boldsymbol{x}_L. \tag{4}$$

In three space dimensions, it is always possible to restrict the number of nonzero β_σ^L to four (in practice, the scheme has been shown to be robust with respect to the choice of these four control volumes, taken close enough to the considered edge). We now define the finite dimensional space $\mathbb{R}^{\mathcal{M}} \times \mathbb{R}^{\mathcal{E}}$ (where an element $v \in \mathbb{R}^{\mathcal{M}} \times \mathbb{R}^{\mathcal{E}}$ is defined by the family of real values $((v_K)_{K\in\mathcal{M}}, (v_\sigma)_{\sigma\in\mathcal{E}})$) and the following subspaces:

- $X^{\mathcal{D}} = \left\{u \in \mathbb{R}^{\mathcal{M}} \times \mathbb{R}^{\mathcal{E}},\ \forall \sigma \in \mathcal{E}_{\rm int}, u_\sigma = \Pi_\sigma(u)\right\}$ (the dimension of $X^{\mathcal{D}}$ is the number of control volumes plus that of boundary edges),
- $X_0^{\mathcal{D}} = \left\{u \in X^{\mathcal{D}},\ \forall \sigma \in \mathcal{E}_{\rm ext}, u_\sigma = 0\right\}$ (the dimension of $X_0^{\mathcal{D}}$ is the number of control volumes),
- $X_{\Gamma_1,0}^{\mathcal{D}} = \left\{\theta \in X^{\mathcal{D}},\ \forall \sigma \in \mathcal{E}_{\rm ext} \cap \Gamma_1, \theta_\sigma = 0\right\}$ (the dimension of $X_{\Gamma_1,0}^{\mathcal{D}}$ is the number of control volumes plus that of boundary edges on Γ_2).

3.1 Discretization of viscous terms

Let us first define a discrete gradient for the elements of $X^{\mathcal{D}}$ on cell $K \in \mathcal{M}$. We set, for any $u \in X^{\mathcal{D}}$ and $K \in \mathcal{M}$:

$$\boldsymbol{\nabla}_K u = \frac{1}{\mathrm{m}_K} \sum_{\sigma \in \mathcal{E}_K} \mathrm{m}_\sigma (u_\sigma - u_K) \boldsymbol{n}_{K,\sigma}.$$

We could construct a discrete gradient with this formula but its use to approximate the diffusive contributions (first terms of the left-hand sides of equations (3a) and (3b)) is not adequate because we cannot construct a coercive form from it, as we do below with a modified gradient in (5). Indeed, for all $\sigma \in \mathcal{E}_K$, we define $R_{K,\sigma} u \in \mathbb{R}$ which may be seen as a consistency error on the normal flux, by:

$$R_{K,\sigma} u = \frac{\sqrt{d}}{d_{K,\sigma}} \left(u_\sigma - u_K - \boldsymbol{\nabla}_K u \cdot (\boldsymbol{x}_\sigma - \boldsymbol{x}_K) \right).$$

(note that $R_{K,\sigma} u = 0$ if u_K and u_σ are the exact values of a linear function at points x_K and x_σ, for all K and σ). We then give the following expression for a discrete gradient of $u \in X^{\mathcal{D}}$ in each cone $C_{K,\sigma}$:

$$\boldsymbol{\nabla}_{K,\sigma} u = \boldsymbol{\nabla}_K u + R_{K,\sigma} u \, \boldsymbol{n}_{K,\sigma},$$

and choose a global discrete gradient as the function $\boldsymbol{\nabla}_{\mathcal{D}} u$ which is such that

$$\boldsymbol{\nabla}_{\mathcal{D}} u(\boldsymbol{x}) = \boldsymbol{\nabla}_{K,\sigma} u, \text{ for a.e. } \boldsymbol{x} \in C_{K,\sigma}, \ \forall K \in \mathcal{M}, \ \forall \sigma \in \mathcal{E}_K.$$

We then get that

$$\int_\Omega \boldsymbol{\nabla}_{\mathcal{D}} u(\boldsymbol{x}) \cdot \boldsymbol{\nabla}_{\mathcal{D}} v(\boldsymbol{x}) \mathrm{d}\boldsymbol{x} = \sum_{K\in\mathcal{M}} \sum_{\sigma\in\mathcal{E}_K} \frac{\mathrm{m}_\sigma d_{K,\sigma}}{d} \boldsymbol{\nabla}_{K,\sigma} u \cdot \boldsymbol{\nabla}_{K,\sigma} v, \ \forall u, v \in X^{\mathcal{D}}. \quad (5)$$

It may then be shown that $\int_\Omega \boldsymbol{\nabla}_{\mathcal{D}} u(\boldsymbol{x}) \cdot \boldsymbol{\nabla}_{\mathcal{D}} v(\boldsymbol{x}) \mathrm{d}\boldsymbol{x}$ defines a symmetric inner product on $X^{\mathcal{D}}$ which provides a good approximation for $\int_\Omega \boldsymbol{\nabla} u(\boldsymbol{x}) \cdot \boldsymbol{\nabla} v(\boldsymbol{x}) \mathrm{d}\boldsymbol{x}$ [4]. It is then possible, expressing u_σ and v_σ for all $\sigma \in \mathcal{E}_{\mathrm{int}}$ thanks to the relations (4), to show that

$$\begin{aligned} &\int_\Omega \boldsymbol{\nabla}_{\mathcal{D}} u(\boldsymbol{x}) \cdot \boldsymbol{\nabla}_{\mathcal{D}} v(\boldsymbol{x}) \mathrm{d}\boldsymbol{x} = \\ &\sum_{K\in\mathcal{M}} \left(\sum_{L\in\mathcal{N}_K} F_{K,L}(u) v_K + \sum_{\sigma\in\mathcal{E}_K\cap\mathcal{E}_{\mathrm{ext}}} F_{K,\sigma}(u)(v_K - v_\sigma) \right), \end{aligned} \quad (6)$$

where for any $K \in \mathcal{M}$, $\mathcal{N}_K \subset \mathcal{M}$ is such that if $L \in \mathcal{N}_K$, then $K \in \mathcal{N}_L$, and for any $K \in \mathcal{M}$ and $L \in \mathcal{N}_K$, $F_{K,L}(u)$ is a linear mapping from $X^{\mathcal{D}}$ to $\mathbb{R}$ such that $F_{K,L}(u) = -F_{L,K}(u)$.

The approximation of $-\int_K \Delta u \mathrm{d}\boldsymbol{x}$ is obtained by letting $v_K = 1$, $v_L = 0$ for $L \neq K$ and $v_\sigma = 0$ for $\sigma \in \mathcal{E}_{\mathrm{ext}}$ in (6):

$$-\int_K \Delta u \mathrm{d}\boldsymbol{x} \simeq \sum_{L\in\mathcal{N}_K} F_{K,L}(u) + \sum_{\sigma\in\mathcal{E}_K\cap\mathcal{E}_{\mathrm{ext}}} F_{K,\sigma}(u),$$

so that we may define an approximate Laplace operator $\Delta_{\mathcal{M}}$ by the constant values $\Delta_K u$ on the cells K:

$$\Delta_K u = \frac{1}{\mathrm{m}_K} \left(\sum_{L\in\mathcal{N}_K} F_{K,L}(u) + \sum_{\sigma\in\mathcal{E}_K\cap\mathcal{E}_{\mathrm{ext}}} F_{K,\sigma}(u) \right). \quad (7)$$

The stencil of the discrete operator is then the set of control volumes M such that there exists $L \in \mathcal{N}_K$ with $F_{K,L}(u)$ depending on u_M. In practice, the equation for a given cell usually concerns the unknowns associated to itself, its neighbours and its neighbours' neighbours. In general, the resulting matrix is not an "M-matrix". Nevertheless, this property is fully recovered when using particular meshes such as, for example, conforming orthogonal parallelepipeds. Indeed, in such a case, locating $\boldsymbol{x}_K$ at the center of gravity of the cell K, the relation $(\boldsymbol{x}_\sigma - \boldsymbol{x}_K)/d_{K,\sigma} = \boldsymbol{n}_{K,\sigma}$ holds. It is then possible to define the second order linear interpolation $\Pi_\sigma(v)$ by $\Pi_\sigma(v) = (d_{L,\sigma}v_K + d_{K,\sigma}v_L)/(d_{L,\sigma} + d_{K,\sigma})$ for all σ such that $\mathcal{M}_\sigma = \{K, L\}$, and for all $v \in X^{\mathcal{D}}$. Using the identity

$$\sum_{\sigma \in \mathcal{E}_K} \mathrm{m}_\sigma (\boldsymbol{x}_\sigma - \boldsymbol{x}_K) \boldsymbol{n}_{K,\sigma}^t = \mathrm{m}_K \mathbb{I}$$

where ^{t} designates the transposition and $\mathbb{I}$ the identity matrix, we obtain, thanks to simple computations:

$$\begin{aligned}\int_\Omega \boldsymbol{\nabla}_{\mathcal{D}} u(\boldsymbol{x}) \cdot \boldsymbol{\nabla}_{\mathcal{D}} v(\boldsymbol{x}) \mathrm{d}\boldsymbol{x} = & \sum_{\sigma \in \mathcal{E}_{\mathrm{int}}, \mathcal{M}_\sigma = \{K,L\}} \frac{\mathrm{m}_\sigma}{d_{K,\sigma} + d_{L,\sigma}} (u_L - u_K)(v_L - v_K) \\ & + \sum_{\sigma \in \mathcal{E}_{\mathrm{ext}}, \mathcal{M}_\sigma = \{K\}} \frac{\mathrm{m}_\sigma}{d_{K,\sigma}} (u_\sigma - u_K)(v_\sigma - v_K).\end{aligned}$$

Then the previous relation leads to define $\mathcal{N}_K$ as the set of the natural neighbours of K, and to define the fluxes by the natural two-point difference scheme, in the same manner as in [3,11]:

$$F_{K,L}(u) = \frac{\mathrm{m}_\sigma}{d_{K,\sigma} + d_{L,\sigma}}(u_K - u_L) \quad \text{for } \sigma \in \mathcal{E}_{\rm int}, \mathcal{M}_\sigma = \{K, L\}$$

$$F_{K,\sigma}(u) = \frac{\mathrm{m}_\sigma}{d_{K,\sigma}}(u_K - u_\sigma) \qquad \text{for } \sigma \in \mathcal{E}_{\rm ext}, \mathcal{M}_\sigma = \{K\}.$$

The classical and cheap 5- and 7-point schemes on rectangular or orthogonal parallelepipedic meshes is then recovered. An advantage can then be taken from this property, by using meshes which consist in orthogonal parallelepipedic control volumes in the main part of the interior of the domain, as we show in the numerical examples.

3.2 Pressure-velocity coupling, mass balance and convective contributions

For all $\boldsymbol{v} \in (X_0^{\mathcal{D}})^d$, we define a discrete divergence operator by:

$$\mathrm{div}_K \boldsymbol{v} = \frac{1}{\mathrm{m}_K} \sum_{\sigma \in \mathcal{E}_K} \mathrm{m}_\sigma \boldsymbol{v}_\sigma \cdot \boldsymbol{n}_{K,\sigma}, \qquad \forall K \in \mathcal{M}.$$

Notice that

$$\mathrm{div}_K \boldsymbol{v} = \sum_{i=1}^{d} (\boldsymbol{\nabla}_K v^{(i)})^{(i)}.$$

We then define the function $\mathrm{div}_{\mathcal{D}} \boldsymbol{v}$ by the relation

$$\mathrm{div}_{\mathcal{D}} \boldsymbol{v}(\boldsymbol{x}) = \mathrm{div}_K \boldsymbol{v}, \text{ for a.e. } \boldsymbol{x} \in K, \ \forall K \in \mathcal{M}.$$

As recalled in the introduction of this paper, a pressure stabilization method is implemented in the mass conservation equation in order to prevent from oscillations of the pressure, as for instance in [2] in the finite element setting, [8], [10] in the finite volume setting. The originality of our approach is that we directly include the stabilizing diffusive pressure flux in the approximated

mass flux, so that it will appear not only (as usual) in the mass equation, but also in the momentum equation through the non-linear convective term. From the mathematical point of view, this helps in obtaining simple estimates on the velocity and pressure, but more importantly, it ensures that the contribution of the discrete non-linear convective term to the kinetic (and thermal) energy balance is zero, just as in the continuous case. Let us define the stabilized mass flux across $\sigma \in \mathcal{E}_{\rm int}$ with $\mathcal{M}_\sigma = \{K, L\}$, by

$$\Phi^\lambda_{K,\sigma}(\boldsymbol{u}, p) = \mathrm{m}_\sigma \left(\boldsymbol{u}_\sigma \cdot \boldsymbol{n}_{K,\sigma} + \lambda_\sigma (p_K - p_L) \right), \tag{8}$$

where $(\lambda_\sigma)_{\sigma \in \mathcal{E}_{\rm int}}$ is a given family of positive real numbers, the choice of which is discussed below. Note that the quantity $\lambda_\sigma(p_K - p_L)$ may be seen as a numerical pressure diffusion flux, and that the overall numerical flux remains conservative, that is, if $\sigma \in \mathcal{E}_{\rm int}$ with $\mathcal{M}_\sigma = \{K, L\}$, then $\Phi^\lambda_{K,\sigma}(\boldsymbol{u}, p) + \Phi^\lambda_{L,\sigma}(\boldsymbol{u}, p) = 0$. We then use this modified flux, in order to define a stabilized centered transport operator which is defined, for all $\boldsymbol{v} \in (X_0^{\mathcal{D}})^d$, $w \in X^{\mathcal{D}}$ and $K \in \mathcal{M}$, by

$$\mathrm{div}^\lambda_K(w, \boldsymbol{u}, p) = \frac{1}{\mathrm{m}_K} \sum_{\sigma \in \mathcal{E}_K \cap \mathcal{E}_{\rm int}, \mathcal{M}_\sigma = \{K,L\}} \Phi^\lambda_{K,\sigma}(\boldsymbol{u}, p) \frac{w_K + w_L}{2}.$$

An interesting remark is that, in the case where the mass balance equation in the control volume K is satisfied, that is:

$$\mathrm{div}^\lambda_K(1, \boldsymbol{u}, p) = \frac{1}{\mathrm{m}_K} \sum_{\sigma \in \mathcal{E}_K \cap \mathcal{E}_{\rm int}} \Phi^\lambda_{K,\sigma}(\boldsymbol{u}, p) = 0,$$

then

$$\sum_{\sigma\in\mathcal{E}_K\cap\mathcal{E}_{\rm int}} \Phi^\lambda_{K,\sigma}(\boldsymbol{u},p)w_K = 0,$$

so that the following relation also holds:

$$\mathrm{m}_K \mathrm{div}^\lambda_K(w,\boldsymbol{u},p) = \sum_{\sigma\in\mathcal{E}_K\cap\mathcal{E}_{\rm int},\mathcal{M}_\sigma=\{K,L\}} \Phi^\lambda_{K,\sigma}(\boldsymbol{u},p)\frac{w_L-w_K}{2}.$$

We shall use this latter form in the practical implementation, in particular in the discretization of the non-linear convection term. Indeed, it is more efficient when computing the Jacobian matrix of the momentum equation, since it avoids summing up values of the same amplitude. When the local grid Reynolds (or Péclet) number is much larger than 1, an upwind scheme must be applied that consists in substituting $\mathrm{div}^\lambda_K(w,\boldsymbol{v},p)$ by

$$\mathrm{div}^{\lambda,\mathrm{up}}_K(w,\boldsymbol{u},p) =$$

$$\frac{1}{\mathrm{m}_K} \sum_{\substack{\sigma\in\mathcal{E}_K\cap\mathcal{E}_{\rm int}\\ \mathcal{M}_\sigma=\{K,L\}}} \Big(\max(\Phi^\lambda_{K,\sigma}(\boldsymbol{u},p),0)w_K + \min(\Phi^\lambda_{K,\sigma}(\boldsymbol{u},p),0)w_L\Big).$$

In both cases, the functions $\mathrm{div}^\lambda_{\mathcal{D}}(w,\boldsymbol{u},p)$ and $\mathrm{div}^{\lambda,\mathrm{up}}_{\mathcal{D}}(w,\boldsymbol{u},p)$ are defined by their constant values in each control volume.

For $u,v\in(X^{\mathcal{D}}_0)^d$, we shall also define the centered vector valued divergence operator $\mathbf{div}^\lambda_{\mathcal{D}}(\boldsymbol{w},\boldsymbol{u},p)$ and $\mathbf{div}^{\lambda,\mathrm{up}}_{\mathcal{D}}(\boldsymbol{w},\boldsymbol{u},p)$ such that the i-th component of $\mathbf{div}^\lambda_{\mathcal{D}}(\boldsymbol{w},\boldsymbol{u},p)$ is equal to $\mathrm{div}^\lambda_{\mathcal{D}}(w_i,\boldsymbol{u},p)$, for $i=1,\ldots,d$, and the same goes

for the upwind divergence.

3.3 Choice for the parameters $(\lambda_\sigma)_{\sigma\in\mathcal{E}_{\rm int}}$

Different strategies can be applied to define the parameters $(\lambda_\sigma)_{\sigma\in\mathcal{E}_{\rm int}}$. Amongst all of them we applied the "cluster stabilization method" [3,11] that consists in constructing a partition of $\mathcal{M}$, denoted $\mathcal{G}$, and set $\lambda_\sigma = \lambda$ if there exists $G \in \mathcal{G}$ (such $G \subset \mathcal{M}$ is called a cluster) with $\mathcal{M}_\sigma \subset G$, otherwise we set $\lambda_\sigma = 0$. Here is an example of such an algorithm: first for all cells K, initialize a new cluster if K and its neighbouring cells do not already belong to a cluster (Figs. 2a,b); then for any remaining isolated cell L, connect it to the closest cluster having the largest number of common edges with L (Fig. 2c).

3.4 Resulting discrete equations

We denote by $T_{b,\mathcal{D}}$ the element $T \in X^{\mathcal{D}}$ such that $T_K = 0$ for all $K \in \mathcal{M}$, $T_\sigma = 0$ for all $\sigma \in \mathcal{E}_{\rm int}$ and all $\sigma \in \mathcal{E}_{\rm ext}$ with $\sigma \subset \Gamma_2$, and, for all $\sigma \in \mathcal{E}_{\rm ext}$ with $\sigma \subset \Gamma_1$,

$$T_\sigma = \frac{1}{\mathrm{m}_\sigma}\int_\sigma T_b(\boldsymbol{x})\mathrm{d}s(\boldsymbol{x}). \tag{9}$$

Let $\mathcal{H}_{\mathcal{M}}(\Omega) \subset L^2(\Omega)$ denote the set of functions which are constant in each $K \in \mathcal{M}$; for any function $q \in \mathcal{H}_{\mathcal{M}}(\Omega)$, we shall denote by q_K its constant value on $K \in \mathcal{M}$. We then define the mapping $P_{\mathcal{M}} : X^{\mathcal{D}} \to \mathcal{H}_{\mathcal{M}}(\Omega)$ by $v \in X^{\mathcal{D}} \mapsto P_{\mathcal{M}}v$ with $P_{\mathcal{M}}v(\boldsymbol{x}) = v_K$ for a.e. $\boldsymbol{x} \in K$ and all $K \in \mathcal{M}$. We also define the mapping $P_{\mathcal{E}} : X^{\mathcal{D}} \to L^2(\Gamma)$ by $v \in X^{\mathcal{D}} \mapsto P_{\mathcal{E}}v$ with $P_{\mathcal{E}}v(\boldsymbol{x}) = v_\sigma$ for a.e. $\boldsymbol{x} \in \sigma$ and all $\sigma \in \mathcal{E}_{\rm ext}$.

Let us then use the previously defined discrete operators to formulate a discrete approximation to problem (3a-3b) :

find $\boldsymbol{u} = (u^{(i)})_{i=1,d} \in (X_0^{\mathcal{D}})^d$, $p \in \mathcal{H}_{\mathcal{M}}(\Omega)$ with $\int_\Omega p(\boldsymbol{x})\mathrm{d}\boldsymbol{x} = \sum_{K\in\mathcal{M}} \mathrm{m}_K p_K = 0$ and $T - T_{b,\mathcal{D}} \in X^{\mathcal{D}}_{\Gamma_1,0}$ such that:

the discrete momentum balance holds:

$$\begin{aligned} &\mathrm{Pr}\int_\Omega \boldsymbol{\nabla}_{\mathcal{D}}\boldsymbol{u} : \boldsymbol{\nabla}_{\mathcal{D}}\boldsymbol{v}\ \mathrm{d}\boldsymbol{x} - \int_\Omega p\ \mathrm{div}_{\mathcal{D}}\boldsymbol{v}\ \mathrm{d}\boldsymbol{x} + \int_\Omega \mathbf{div}^{\lambda}_{\mathcal{D}}(\boldsymbol{u},\boldsymbol{u},p)\cdot P_{\mathcal{M}}\boldsymbol{v}\ \mathrm{d}\boldsymbol{x} \\ &-\mathrm{Ra}\,\mathrm{Pr}\int_\Omega P_{\mathcal{M}}T\ \boldsymbol{e}_3\cdot P_{\mathcal{M}}\boldsymbol{v}\ \mathrm{d}\boldsymbol{x} = \int_\Omega \boldsymbol{f}\cdot P_{\mathcal{M}}\boldsymbol{v}\ \mathrm{d}\boldsymbol{x},\ \forall \boldsymbol{v}\in (X_0^{\mathcal{D}})^d, \end{aligned} \tag{10}$$

the energy balance holds:

$$\begin{aligned} &\int_\Omega \boldsymbol{\nabla}_{\mathcal{D}}T\cdot\boldsymbol{\nabla}_{\mathcal{D}}\theta\ \mathrm{d}\boldsymbol{x} + \int_\Omega \mathrm{div}^{\lambda}_{\mathcal{D}}(T,\boldsymbol{u},p)P_{\mathcal{M}}\theta\ \mathrm{d}\boldsymbol{x} \\ &= \int_\Omega g\ P_{\mathcal{M}}\theta\ \mathrm{d}\boldsymbol{x} - \int_{\Gamma_2} q_b P_{\mathcal{E}}\theta\ \mathrm{d}s,\ \forall\theta\in X^{\mathcal{D}}_{\Gamma_1,0}, \end{aligned} \tag{11}$$

the mass balance holds:

$$\mathrm{div}^{\lambda}_{\mathcal{D}}(1,\boldsymbol{u},p) = 0 \text{ a.e. in } \Omega. \tag{12}$$

We then deduce from (10) the d discrete equations of the conservation of momentum in the control volume K, letting $v^{(i)} = 1$ in K, and 0 otherwise.

These equations read, in vector form:

$$\begin{aligned} &\mathrm{m}_K \Delta_K \boldsymbol{u} + \sum_{\substack{\sigma \in \mathcal{E}_{\mathrm{int}} \\ \mathcal{M}_\sigma = \{M,L\}}} \mathrm{m}_\sigma \beta_\sigma^K (p_M - p_L)\ \boldsymbol{n}_{L,\sigma} \\ &+ \sum_{\substack{\sigma \in \mathcal{E}_K \cap \mathcal{E}_{\mathrm{int}} \\ \mathcal{M}_\sigma = \{K,L\}}} \Phi_{K,\sigma}^{\lambda}(\boldsymbol{u}, p) \frac{\boldsymbol{u}_K + \boldsymbol{u}_L}{2} - \mathrm{Ra}\,\mathrm{Pr}\ \mathrm{m}_K T_K \boldsymbol{e}_3 = \int_K \boldsymbol{f}\ \mathrm{d}\boldsymbol{x} \end{aligned} \tag{13}$$

(where $\Delta_K \boldsymbol{u}$ is the vector valued discrete Laplace operator defined by (7) for each of its component). Similarly, we deduce from (11) the discrete equation of the conservation of energy in the control volume K, letting $\theta = 1$ in K, and 0 otherwise. This equation reads:

$$\mathrm{m}_K \Delta_K T + \sum_{\substack{\sigma \in \mathcal{E}_K \cap \mathcal{E}_{\mathrm{int}} \\ \mathcal{M}_\sigma = \{K,L\}}} \Phi_{K,\sigma}^{\lambda}(\boldsymbol{u}, p) \frac{T_K + T_L}{2} = \int_K g \mathrm{d}\boldsymbol{x}. \tag{14}$$

Recall that, for all $K \in \mathcal{M}$, and all $\sigma \in \mathcal{E}_K$ such that $\sigma \subset \Gamma_1$, the following Dirichlet boundary condition (9) is imposed. We deduce from (11) the relation imposed by the Neumann boundary condition for the thermal flux, letting $\theta_\sigma = 1$ and 0 otherwise, for some $\sigma \in \mathcal{E}_K$ with $\sigma \subset \Gamma_2$:

$$F_{K,\sigma}(T) = \int_\sigma q_b(\boldsymbol{x}) \mathrm{d}s(\boldsymbol{x}). \tag{15}$$

Note that the above relation is natural, accounting for the fact that $F_{K,\sigma}(T)$ approximates the heat flux at the edge σ. Finally, we write (12) in a given control volume K:

$$\sum_{\sigma \in \mathcal{E}_K \cap \mathcal{E}_{\mathrm{int}}} \Phi_{K,\sigma}^{\lambda}(\boldsymbol{u}, p) = 0. \tag{16}$$

290

291 *3.5 Some mathematical properties*

292 The system of discrete equations (13-16) appears as a system of non-linear
293 equations. The mathematical proof of the existence of at least a solution can
294 be shown in the particular case $T_b = 0$ and $q_b = 0$, which we consider in this
295 section. Indeed, in this case, we can show some a priori bounds on T and $\boldsymbol{u}$.
296 We first let $\theta = T$ in (11). Using the relation

$$\int_\Omega \mathrm{div}_{\mathcal{D}}^{\lambda}(T, \boldsymbol{u}, p)\ P_{\mathcal{M}} T\ \mathrm{d}\boldsymbol{x} = 0,$$

297 which results from (12), we get

$$\|\boldsymbol{\nabla}_{\mathcal{D}} T\|_{L^2(\Omega)^d}^2 = \int_\Omega g\ P_{\mathcal{M}} T\ \mathrm{d}\boldsymbol{x}.$$

298 Thanks to a discrete Poincaré inequality which follows from [5, Lemma 5.3],
299 we get that there exists C_T, only depending on the regularity of the mesh and
300 on g, but not on the size of the mesh, such that

$$\|\boldsymbol{\nabla}_{\mathcal{D}} T\|_{L^2(\Omega)^d} \leq C_T.$$

301 We then let $\boldsymbol{v} = \boldsymbol{u}$ in (10). We get, thanks to (8) and (12),

$$\begin{aligned}
&\mathrm{Pr}\|\boldsymbol{\nabla}_{\mathcal{D}} \boldsymbol{u}\|_{(L^2(\Omega)^d)^d}^2 + \sum_{\substack{\sigma \in \mathcal{E}_{\mathrm{int}} \\ \mathcal{M}_\sigma = \{K,L\}}} \mathrm{m}_\sigma \lambda_\sigma (p_L - p_K)^2 \\
&= \int_\Omega (\boldsymbol{f} + \mathrm{Ra}\,\mathrm{Pr}\ P_{\mathcal{M}} T \boldsymbol{e}_3) \cdot P_{\mathcal{M}} \boldsymbol{u}\ \mathrm{d}\boldsymbol{x}.
\end{aligned}$$

Again using the Poincaré inequality, we conclude that there exists $C_{\boldsymbol{u}}$, only depending on the regularity of the mesh, on Ra, Pr, f and g, but not on the size of the mesh, such that

$$\|\boldsymbol{\nabla}_{\mathcal{D}}\boldsymbol{u}\|_{(L^2(\Omega)^d)^d} \leq C_{\boldsymbol{u}}.$$

Hence, using the topological degree method, we can prove the existence of at least one solution. Moreover, these inequalities are then sufficient to get compactness properties, which show that, from a sequence of discrete solutions with the space step tending to zero, we can extract a converging subsequence, for suitable norms. Then we can prove that the limit of this subsequence has a sufficient regularity, in relation with the weak sense provided by (3). It is then possible to pass to the limit on (11), (10) and (12), using test functions which are interpolation of regular ones. We then get that the limit of the converging subsequence satisfies (3).

4 Numerical validation

The set of non-linear equations (13-16) is solved by an under-relaxed Newton method where the unknowns are the velocity $\boldsymbol{u}_K$, the pressure p_K and the temperature T_K and T_σ for all $K \in \mathcal{M}$ and $\sigma \in \mathcal{E}_{\text{ext}} \cap \Gamma_2$. The solutions of the linear systems are computed with a parallel Generalized Minimal RESidual method provided by the scalable linear solvers package *HYPRE* with a pre-conditioning based on the block Jacobi iLU factorization carried out by *Euclid*

[6].

4.1 Analytical solutions

We consider two closed cavities, cubic or cone-shaped, in which the fluid flow and the heat transfer are known *a priori*. Let $p_{\rm ref}(\boldsymbol{x})$, $\boldsymbol{u}_{\rm ref}(\boldsymbol{x})$ and $T_{\rm ref}(\boldsymbol{x})$ be the pressure, the velocity satisfying the mass equation (1c) and the temperature field. Since the exact solutions are known, the right-hand sides $\boldsymbol{f}(\boldsymbol{x})$ and $g(\boldsymbol{x})$ in equations (13) and (14) are chosen as the residuals of the Navier-Stokes (Eq. 1a) and energy equations (Eq. 1b) with $\boldsymbol{u}(\boldsymbol{x}) \equiv \boldsymbol{u}_{\rm ref}(\boldsymbol{x})$, $p(\boldsymbol{x}) \equiv p_{\rm ref}(\boldsymbol{x})$ and $T(\boldsymbol{x}) \equiv T_{\rm ref}(\boldsymbol{x})$. We denote by $(n_i)_{i=1,\cdots,3}$ the number of cells in directions $(\boldsymbol{e}_i)_{i=1,\cdots,3}$. For any regular function $\psi(\boldsymbol{x}) \in \{(u^{(i)}(\boldsymbol{x}))_{i=1,\cdots,3}, p(\boldsymbol{x}), T(\boldsymbol{x})\}$, the relative accuracy of the scheme is measured by $\|\psi - \psi_{\rm ref}\|_\infty / \|\psi_{\rm ref}\|_\infty$, $\|\psi - \psi_{\rm ref}\|_2 / \|\psi\|_2$ and $\|\psi - \psi_{\rm ref}\|_{H_1} / \|\psi_{\rm ref}\|_{H_1}$, with $\|\psi - \psi_{\rm ref}\|_\infty = \max_{K\in\mathcal{M}} |\psi_K - \psi_{\rm ref}(\boldsymbol{x}_K)|$, $\|\psi - \psi_{\rm ref}\|_2 = \sqrt{\sum_{K\in\mathcal{M}} {\rm m}_K (\psi_K - \psi_{\rm ref}(\boldsymbol{x}_K))^2}$ and $\|\psi - \psi_{\rm ref}\|_{H_1} = \sqrt{\sum_{i=1}^d (\|\boldsymbol{\nabla}^{(i)}_{\mathcal{D},\mathcal{M}} \psi - \boldsymbol{\nabla}^{(i)} \psi_{\rm ref}\|_2)^2}$

Three kinds of meshes are studied for the unit cubic enclosure. The first one is the simplest mesh consisting of regular parallelepipeds where $\boldsymbol{x}_K$ is located at the gravity center of the cell. The second one (Fig. 3a) is constructed by a smooth mapping between the logical mesh and the spatial coordinates [1]. The vertices $\boldsymbol{x}_{\rm s}(i,j,k) = \left(\boldsymbol{x}^{(l)}_{\rm s}(i,j,k)\right)_{l=1,\cdots,3}$ of the elementary distorted cubes are defined by: $\forall (i,j,k) \in N([1,n_1+1]) \times N([1,n_2+1]) \times N([1,n_3+1])$,

$$\boldsymbol{x}_{\rm s}^{(1)}(i,j,k) = 1 - \cos\left(\frac{\pi(i-1)}{2n_1}\right)$$
$$\boldsymbol{x}_{\rm s}^{(2)}(i,j,k) = \frac{(j-1)}{n_2} + 0.1\sin\left(\frac{2\pi(j-1)}{n_2}\right)\sin\left(\frac{2\pi(k-1)}{n_3}\right)$$
$$\boldsymbol{x}_{\rm s}^{(3)}(i,j,k) = \frac{(k-1)}{n_3} + 0.1\sin\left(\frac{2\pi(j-1)}{n_2}\right)\sin\left(\frac{2\pi(k-1)}{n_3}\right)$$

and $(\boldsymbol{x}_K)_{K\in\mathcal{M}}$ are located at the gravity centers of the cells. The third and last mesh for the cubic cavity (Fig. 3b) is based on parallelepipeds where $\boldsymbol{x}_K$ is again at the gravity center of K. Then, each vertex $\boldsymbol{x}_{\rm s}$ of the cells is randomly displaced in the $l = 1, \cdots, 3$ space directions of a magnitude at most equal to 90% of the quantity $\min_{K\in\mathcal{M}} |\boldsymbol{x}_{\rm s}^{(l)} - \boldsymbol{x}_K^{(l)}|$. Unlike the previous mesh, which consisted of hexahedra with plane faces, the four edges of a face are now not included into a same plane, with the exception of edges which belong to the boundaries of the cubic domain.

The conic-shaped cavity is bounded by the lateral surface $((x^{(1)} - 0.5)^2 + (x^{(2)} - 0.5)^2 = ((6 - 5x^{(3)})/12)^2$ for $x^{(3)} \in [0, 1]$ and by two plane discs $(x^{(1)} - 0.5)^2 + (x^{(2)} - 0.5)^2 \leq 1/4$ for $x^{(3)} = 0$ and $(x^{(1)} - 0.5)^2 + (x^{(2)} - 0.5)^2 \leq 1/12^2$ for $x^{(3)} = 1$. The mesh of this enclosure is based on cubes which were only cut to match the lateral curved boundary. Thus, the mesh error tends to zero quadratically with respect to the mesh size. Remark that the resulting boundary cells having a volume less than $0.1 \prod_{i=1}^{d} 1/n_i$ are merged into adjacent cells in order to avoid too large differences of volumes between adjacent cells that may deteriorate the numerical accuracy. To illustrate the mesh at the boundaries (Fig. 3c), the polyhedra K have to be divided into tetrahedrons by using the nodes $\boldsymbol{x}_K$, $\boldsymbol{x}_\sigma$, and two successive vertices which define the edge $\sigma \in \mathcal{E}_K$.

We are first interested in the pure diffusive problem of a scalar variable (Eq. (14) with $\boldsymbol{u} = 0$) where $\Gamma_1 = \Gamma$ and $\Gamma_2 = \{\emptyset\}$. It was first checked that the errors obtained with a linear analytical solution on the different meshes and cavities are of the order of the computer accuracy, even for the coarsest grids. The next analytical test consists in choosing the reference solution $T_{\text{ref}}(x^{(1)}, x^{(2)}, x^{(3)}) = \sin(\pi x^{(1)}) \cos(\pi x^{(2)}) \cos(\pi x^{(3)})$ with appropriate Dirichlet boundary conditions (Fig. 4a-c). The orders of convergence are evaluated by the values of the mean slopes of the curves representing the relative errors as a function of the mesh size (Tab. 1). The accuracy of the scheme is therefore close to 2 when considering the L^2-norm and it slightly decreases with the L^∞-norm but always remains larger than 1.5. As expected, the order of convergence for the gradients (H^1-norm) is 1.

We now examine the convergence behavior of the isothermal Navier-Stokes equations by setting $\boldsymbol{u}_{\text{ref}}(\boldsymbol{x}) = \boldsymbol{\nabla} \wedge \sum_{i=1}^{d} (4x^{(1)}(x^{(1)}-1))^3 (4x^{(2)}(x^{(2)}-1))^4 (4x^{(3)}(x^{(3)}-1))^5 \boldsymbol{e}_i$ and $p_{\text{ref}}(\boldsymbol{x}) = \cos(\pi x^{(1)}) \cos(\pi x^{(2)}) \cos(\pi x^{(3)})$ in (Eq. 3a) with $\text{Pr} = 1$ and $\text{Ra} = 0$ (note that the dimensionless writing of the equations is meaningless because the current reference velocity is related to the thermal diffusivity which never appears for isothermal problems. Another velocity reference should be used, based on the viscous diffusivity so that the Péclet number was replaced by the Reynolds number, $\text{Re} = 1$). The table (2) indicates that the convergence rates of the velocity components are larger than 1.90 on the three finer meshes when the relative error is based on the L^2-norm and first order accurate for the pressure for distorted meshes. In accordance with the diffusion problem when the L^∞-norm is used, the orders of convergence slightly decrease for the velocity but a convergence rate larger than 1.6 is still observed. The convergence

rates of the gradients are better than the expected first order. Unsurprisingly, the L^∞ and H^1-norms of the pressure do not tend to zero with the mesh size because it simply appears in the momentum equation as lagrangian multiplier of the mass equation. Thus the only guaranteed convergence for the pressure is based on the L^2-norm.

4.2 Natural convection problem

We consider an air filled unit-cubic enclosure with isolated walls except the two face to face vertical isothermal surfaces at $x^{(1)} = 0$ and 1. The governing fluid flow equations are solution of system (1) and (2) with $\boldsymbol{f}(\boldsymbol{x}) = \boldsymbol{0}$, $g(\boldsymbol{x}) = 0$, $q_b(\boldsymbol{x}) = 0$, $T(0, x^{(2)}, x^{(3)}) = -0.5$ and $T(1, x^{(2)}, x^{(3)}) = 0.5$. The Prandtl and Rayleigh numbers are fixed to $\mathrm{Pr} = 0.71$ and $\mathrm{Ra} = 10^7$ and the stabilization parameter is chosen equal to $\lambda_\sigma = 10^{-8}$ in the mass equation (see relation (8)). Because very small boundary layers take place along the walls, the mesh size is non-uniformly distributed in each direction $l \in [1, d]$: $\forall (i,j,k) \in N([1, n_1 + 1]) \times N([1, n_2 + 1]) \times N([1, n_3 + 1])$, $\boldsymbol{x}_{\mathrm{s}}^{(l)}(i,j,k) = \left(1 - \cos \dfrac{\pi(i\delta_{l1} + j\delta_{l2} + k\delta_{l3} - 1)}{n_l}\right)/2$. To also study the effect of non-cubic meshes, the coordinates of the previous defined vertices are randomly displaced of a magnitude at most of $0.9 \min_{K \in \mathcal{M}} |\boldsymbol{x}_{\mathrm{s}}^{(l)} - \boldsymbol{x}_K^{(l)}|$, for $l \in [1, d]$. Table (5) presents the maxima of the velocity components, the average Nusselt number on the isothermal walls and their relative differences with respect to reference data [12]. For cubic meshes and the $\|.\|_\infty$-norm, the scheme seems to be second order at least between $n_i = 40$ and 60 where the relative gap is then divided by about 2 or more. Remark that the results are quite accurate and depart from less than 1% from the reference values when $n_i = 60$. The second order accuracy of numerical solutions is also obtained for randomly

perturbated meshes except for the third velocity component where the convergence order is rather difficult to define. Although $e(u^{(2)})$ is large, it can be noticed firstly that its value is divided by 4 between $n_i = 20$ and 40 and secondly that the corresponding reference value is smaller than the other velocity components, about 10 times smaller in comparison with $u^{(3)}$.

5 Conclusion

In this paper we presented a new scheme which is well suited for the simulation of incompressible viscous flows on irregular and non-conforming grids. This possibility seems to open a large field of new applications (grid refinement as a function of an *a posteriori* error computation, free boundaries, ...). We emphasize that the convergence of the scheme may be proven mathematically, and that the obtained numerical results are accurate. Although we presented this scheme in the steady case, its extension to transient regimes is straightforward. In this latter case, one should consider optimizing the linear solving step by using suitable projection algorithms.

References

[1] J. Breil, P.-H. Maire, A cell-centered diffusion scheme on two-dimensional unstructured meshes, J. Comput. Phys. 224 (2007) 785–823.

[2] F. Brezzi, J. Pitkäranta, On the stabilization of finite element approximations of the Stokes equations, Efficient solutions of elliptic systems (Kiel, 1984), Notes Numer. Fluid Mech., 10, 11–19, Vieweg, Braunschweig.

[3] E. Chénier, O. Touazi, R. Eymard, Numerical results using a colocated finite-volume scheme on unstructured grids for incompressible flows, Num. Heat

Transfer, part B 49 (2006) 1–18.

[4] R. Eymard and R. Herbin. A new colocated finite volume scheme for the incompressible Navier-Stokes equations on general non matching grids, Comptes rendus Mathématiques de l'Académie des Sciences, 344(10) (2007) 659–662.

[5] R. Eymard, T. Gallouët and R. Herbin, Discretization schemes for anisotropic diffusion problems on general nonconforming meshes, submitted, see also `http://hal.archives-ouvertes.fr`

[6] HYPRE 2.0.0, Copyright (c) 2006 The Regents of the University of California. Produced at the Lawrence Livermore National Laboratory. Written by the HYPRE team. UCRL-CODE-222953. All rights reserved.
URL `http://www.llnl.gov/CASC/hypre/`

[7] D. Kershaw, Differencing of the diffusion equation in lagrangian hydrodynamic codes, J. Comput. Phys. 39(2) (1981) 375–395.

[8] S. Nägele, G. Wittum, On the influence of different stabilisation methods for the incompressible Navier-Stokes equations, J. Comput. Phys. 224 (2007) 100–116.

[9] S. Patankar, Numerical Heat Transfer and Fluid Flow, Series in Computational Methods in Mechanics and Thermal Sciences, Mc Graw Hill, 1980.

[10] C. Rhie, W. Chow, Numerical study of the turbulent flow past an airfoil with trailing edge separation, AIAA J. 21 (1983) 1523–1532.

[11] O. Touazi, E. Chénier, R. Eymard, Simulation of natural convection with the collocated clustered finite volume scheme, Computers & Fluids, DOI: 10.1016/j.compfluid.2007.09.006, Article in Press.

[12] E. Tric, G. Labrosse, M. Betrouni, A first incursion into the 3D structure of natural convection of air in a differentially heated cubic cavity, from accurate numerical solutions, Int. J. Heat Mass Transfer 43 (2000) 4043–4056.

List of Tables

List of Figures

	Cubic enclosure			Truncated conic
	cubic meshes	smooth meshes	random meshes	enclosure
L^2-norm	2 (2)	1.95 (1.97)	1.79 (1.93)	1.97 (1.99)
L^∞-norm	1.99 (2)	1.80 (1.68)	1.66 (1.88)	1.81 (1.55)
H^1-norm	2 (2)	1.49 (1.28)	1.11 (1.07)	1.46 (1.46)

Table 1

		Cubic meshes	Smooth meshes	Random meshes
L^2	$u^{(1)}$	2 (2)	1.91 (1.98)	1.71 (1.91)
	$u^{(2)}$	1.99 (2)	1.93 (1.98)	1.73 (1.90)
	$u^{(3)}$	2 (2)	1.92 (1.98)	1.76 (1.90)
	p	2 (2)	1.08 (0.76)	0.80 (0.91)
L^∞	$u^{(1)}$	2 (2)	1.64 (2)	1.52 (1.80)
	$u^{(2)}$	1.75 (1.78)	1.37 (1.64)	1.56 (1.69)
	$u^{(3)}$	1.88 (1.74)	1.53 (1.59)	1.62 (1.82)
	p	1.72 (1.93)	$--$	$--$
H^1	$u^{(1)}$	1.98 (2)	1.77 (1.85)	1.34 (1.29)
	$u^{(2)}$	2 (2)	1.78 (1.84)	1.33 (1.25)
	$u^{(3)}$	1.95 (1.99)	1.74 (1.83)	1.31 (1.23)
	p	1.91 (1.97)	$--$	$--$

Table 2

Mesh types	n_i	$\|u^{(1)}\|_\infty$	$e(u^{(1)})$	$\|u^{(2)}\|_\infty$	$e(u^{(2)})$	$\|u^{(3)}\|_\infty$	$e(u^{(3)})$	Nu	e(Nu)
cubic	20	$333,23$	-13%	$70,959$	-15%	$767,01$	-0.15%	$16,380$	0.23%
	30	$371,89$	-3.1%	$79,105$	-5.1%	$761,11$	-0.91%	$16,366$	0.14%
	40	$377,71$	-1.6%	$81,097$	-2.7%	$761,15$	-0.91%	$16,361$	0.11%
	50	$380,19$	-0.95%	$82,234$	-1.4%	$767,25$	-0.11%	$16,357$	0.086%
	60	$380,47$	-0.88%	$82,615$	-0.93%	$767,90$	-0.031%	$16,353$	0.065%
Random	20	$497,85$	30%	$363,48$	340%	$869,95$	13%	$16,023$	-2.0%
	30	$419,43$	9.3%	$276,63$	230%	$777,25$	1.2%	$16,198$	-0.88%
	40	$400,18$	4.3%	$151,27$	81%	$779,93$	1.5%	$16,259$	-0.51%
[12]		$383,8357$	0%	$83,3885$	0%	$768,1393$	0%	$16,3427$	0%

Table 3

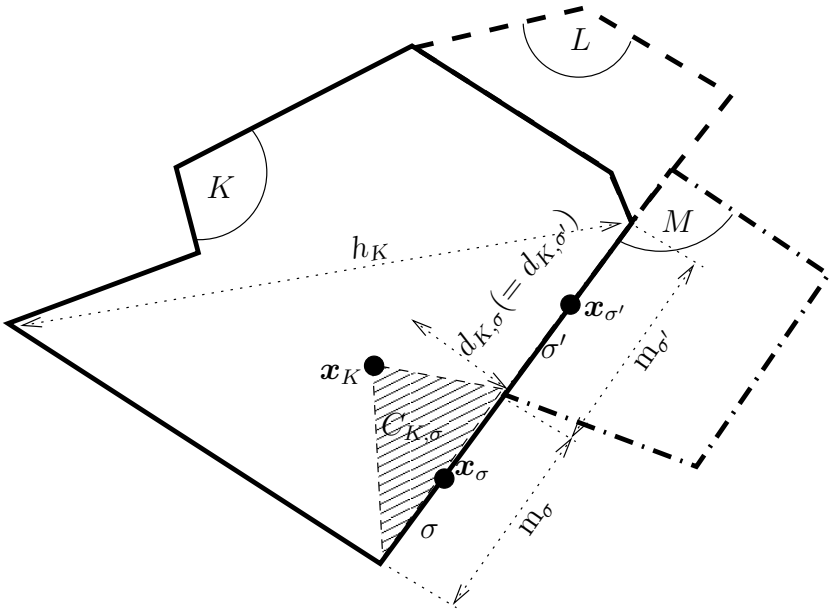
L
K
M
h_K
$d_{K,\sigma'} (= d_{K,\sigma'})$
$x_{\sigma'}$
x_K
σ'
$m_{\sigma'}$
$C_{K,\sigma}$
x_σ
σ
m_σ

Fig. 1.

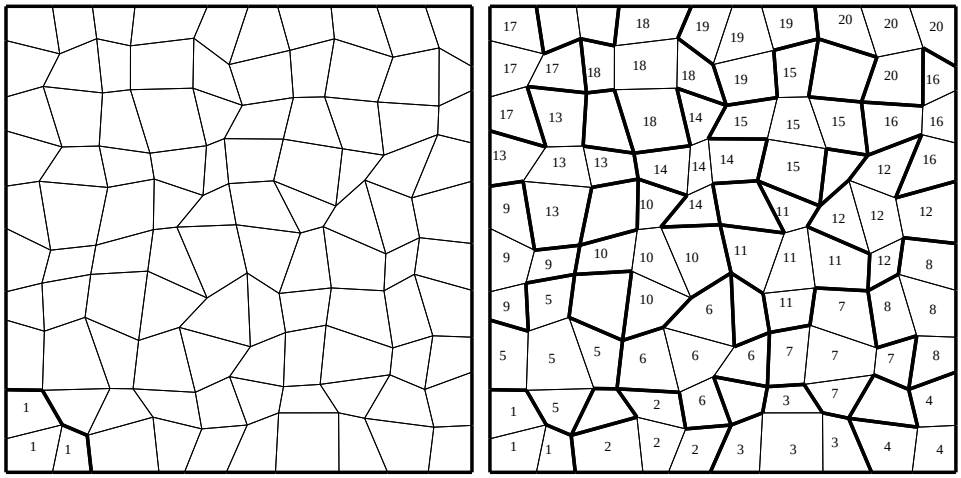

a. b.

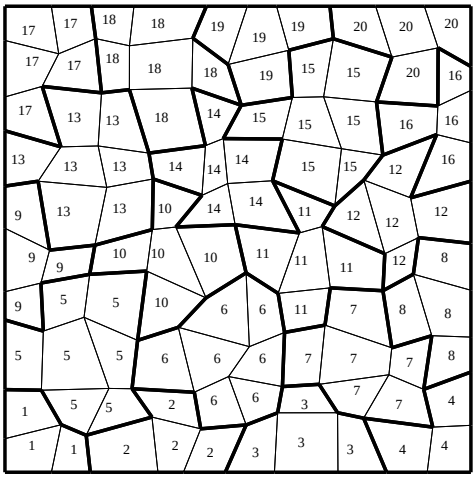

c.

Fig. 2.

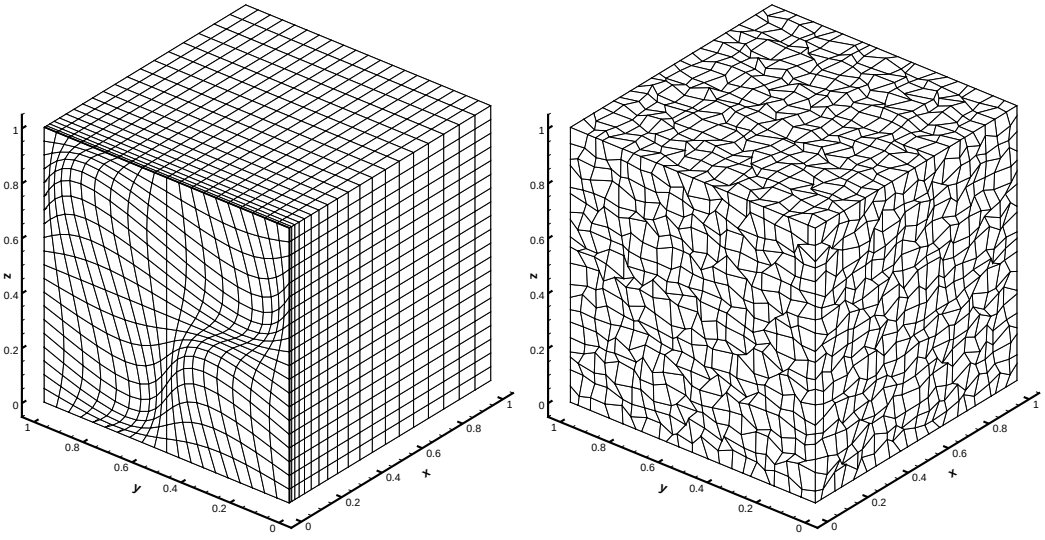

a. b.

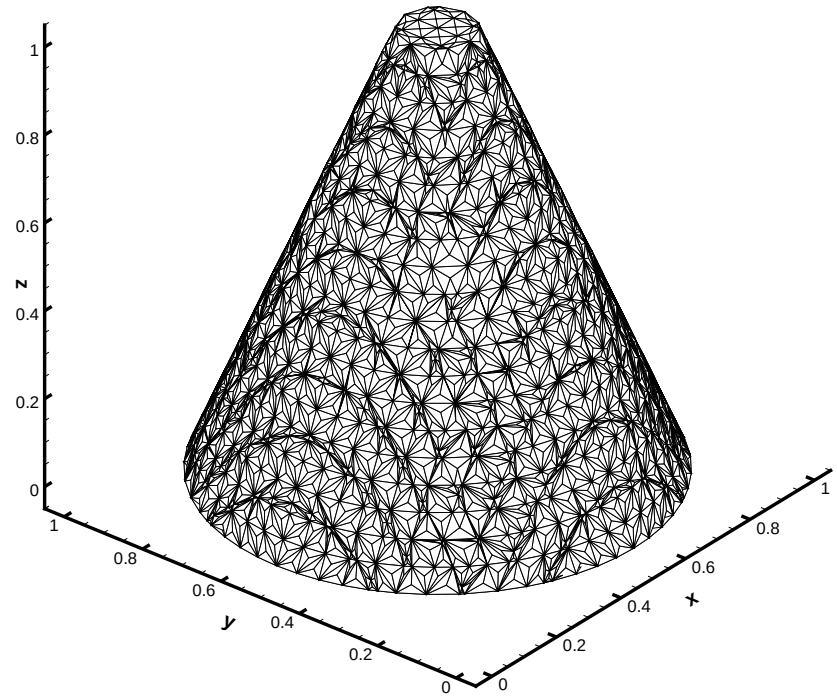

c.

Fig. 3.

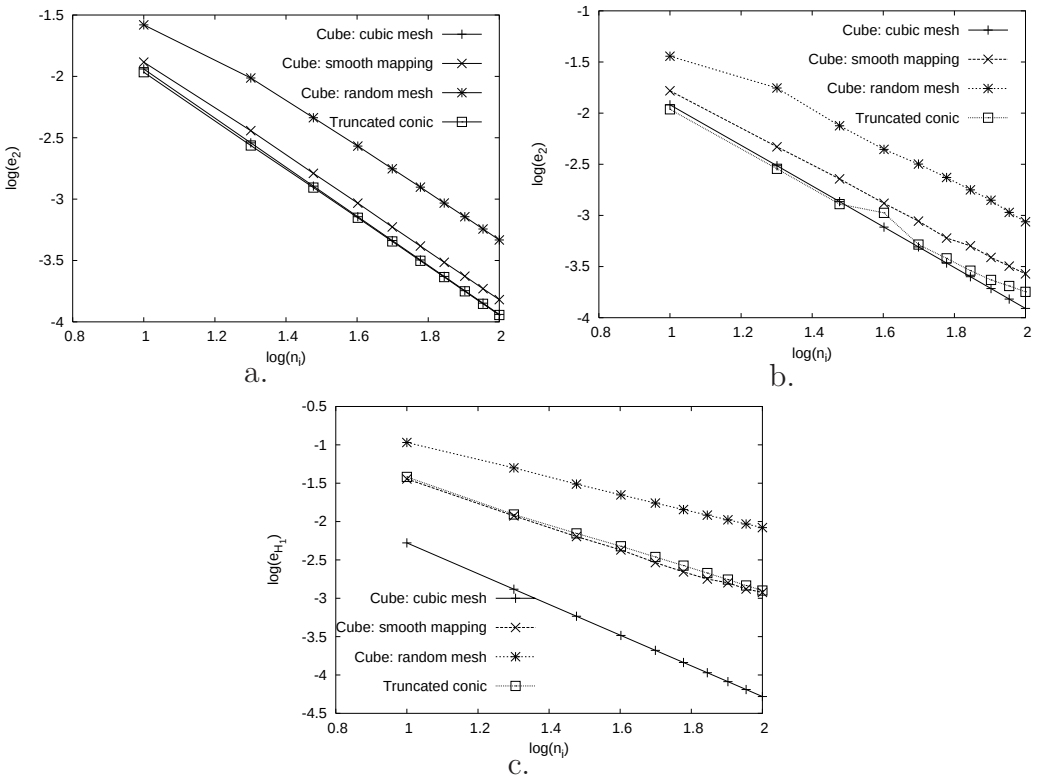
Cube: cubic mesh
Cube: smooth mapping
Cube: random mesh
Truncated conic
log(e2)
log(nl)
a.
b.
log(eH1)
c.

Fig. 4.